

Title No. 114-S71

# Size Effect on Punching Strength of Reinforced Concrete Slabs with and without Shear Reinforcement

by Abdullah Dönmez and Zdeněk P. Bažant

*A design equation for punching shear strength  $v_c$  is developed based on a refined statistical analysis of the ACI 445 database with 440 tests supplemented by finite element (FE) analysis using microplane model M7. Database filtering leads to data subsets in which the averages of secondary variables, such as steel ratio and shape parameters, in subsequent intervals of size  $d$  (or slab depth) are almost constant. The resulting trend of the interval means of  $v_c$  reveals that the slope of  $\log v_c$  versus  $\log d$  through the practical size range is milder, but not much milder, than  $-1/2$ , and that the trend fits the energetic size effect factor endorsed by ACI Committee 446. The design equation with size effect is verified and calibrated by least-square multivariate regression of the database, with weights compensating for the crowding or scarcity of data in parts of the range. The size effect factor is also verified by FE fitting of available broader-range data series.*

**Keywords:** design codes; failure; finite element analysis; optimum data fitting; punching shear; quasibrittle fracture; reinforced concrete; size effect; statistical analysis.

## INTRODUCTION

Although concrete is not plastic, the shear strength of beams and slabs has traditionally been analyzed according to plastic limit analysis. In this analysis, the nominal strength  $v_c$  of geometrically similar structures, defined as the load capacity (or maximum load) divided by the area of a characteristic (homologous) cross section, is independent of structure size  $D$ . This is the case of no size effect. However, if the structural failure is due to fracture or localization of cracking damage, which is typical of concrete,  $v_c$  decreases with  $D$ , which is called the size effect. There are two type of size effects: 1) statistical, due to material strength randomness, which occurs when a macrocrack initiates dynamically from one of many possible places of random strength, as described by the weakest link model and Weibull theory; and 2) energetic (that is, deterministic), which occurs when a large crack grows in a stable manner prior to reaching the maximum load (in which case the material randomness affects only the coefficient of variation of  $v_c$ , and the size effect is due to energy release rate increasing with structure size). The shear failures of reinforced concrete are generally of Type 2, which is the type occurring in structures with a deep notch or a deep stress-free crack formed stably before reaching the maximum load (while Type I size effect is that which occurs in structures that fail right at crack initiation from a smooth surface).<sup>1</sup>

The plastic limit analysis, which underlies the concrete design codes, gives realistic results for relatively small structures used in most laboratory testing. The reason is that the size  $l_0$  of the fracture process zone is in concrete very large—approximately 0.5 m (1.64 ft) (compared to a few micrometers [ $1 \mu\text{m}$  ( $3.9 \times 10^{-5}$  in.)] for metals or fine

grained ceramics). This implies that, at maximum load, the distributed cracking cannot localize into one dominant crack prior to maximum load and, thus, the size effect must be negligible for small structures. The size effect becomes strong only when the structure is sufficiently larger than  $l_0$ . Consequently, extending the current code provisions to large sizes is relatively easy—it suffices to multiply the  $v_c$  value according to the current code, based on limit analysis, with the proper size effect factor, which is approximately 1 for small structure sizes. Herein, it is proposed how to do it for punching shear.

The literature on punching shear has become extensive and includes many significant contributions.<sup>1-20</sup> Their discussions would be superfluous because an excellent review is found in the report by ACI Subcommittee 445-C.<sup>21</sup> The ACI 445-C database for punch failures is used herein; refer to Fig. 1, which shows the nominal punching shear strength

$$v_c = \frac{V_c}{b_o d} \quad (1)$$

normalized by mean concrete strength  $f_c$  as a function of slab depth  $d$ , in comparison with the curves of  $\log v_c/f_c^{1/2}$  (for Eurocode  $\log v_c/f_c^{1/3}$ ) versus  $\log d$  according to design codes;  $d$  is the distance from the compression face to the centroid of flexural reinforcement and is slightly smaller than slab thickness  $h$  (for two-way slabs, this centroid is considered to be the average depth of the centers of flexural reinforcements for both sides,  $d = (d_x + d_y)/2$ );  $V_c$  is load capacity due to concrete; and  $b_o$  is control perimeter, calculated at distance  $d/2$  from the column face. Note that the strength in Eq. (1) is not the design strength, because the material safety factors are not included.

The database for the punch failures, repeated in all four diagrams in Fig. 1, contains the results of 440 tests reported in 60 experimental studies conducted in laboratories worldwide. The slabs had square, rectangular, circular, or octagonal simply supported boundaries. The depths  $d$  in the database range from 30 to 668 mm (1.18 to 26.29 in.); the mean concrete strength  $f_c$  from 8 to 118 MPa (1160 to 17,114 psi), and the longitudinal reinforcement ratio  $\rho$  from 0.1% to 7.3%. The data points in Fig. 1 show very high scatter, but the scatter is due not only to inevitable randomness but also, and largely, to inevitable sampling bias.

*ACI Structural Journal*, V. 114, No. 4, July-August 2017.

MS No. S-2016-076.R2, doi: 10.14359/51689719, was received October 17, 2016, and reviewed under Institute publication policies. Copyright © 2017, American Concrete Institute. All rights reserved, including the making of copies unless permission is obtained from the copyright proprietors. Pertinent discussion including author's closure, if any, will be published ten months from this journal's date if the discussion is received within four months of the paper's print publication.

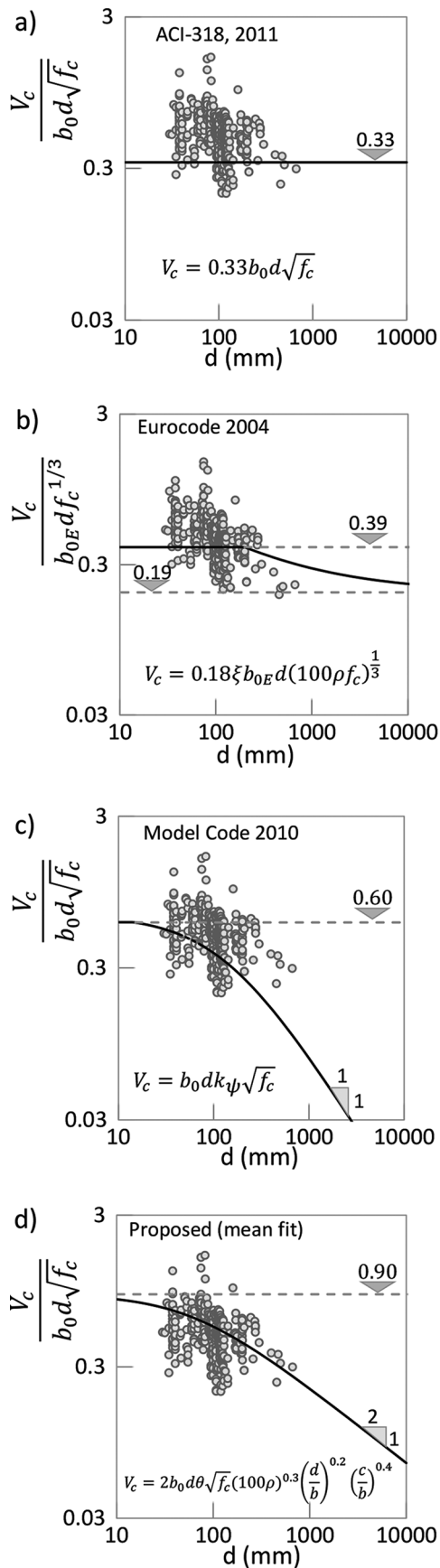


Fig. 1—Normalized strength comparisons among provisions of: (a) ACI ( $\times 12$  for psi); (b) Eurocode ( $\times 5.25$  for psi); (c) Model Code; and (d) proposed. (Note: 1 mm = 0.0394 in.)

The objectives of this study are: 1) filter the inevitable sampling bias from the existing experimental database<sup>21</sup> to reveal the basic size effect trend; 2) propose an improved equation for  $v_c$  that includes the size effect, avoiding insufficient (or uneconomic) safety (or capacity reduction) factors; and 3) calibrate and validate the size effect by weighted multivariate regression.

It is important to realize that, aside from the load factors and understrength factor specified by the design code, additional safety margins are implied in the code by setting the design formula not at the mean of the test data but at its lower margin, and by designing for a reduced material strength that is typically approximately 30% lower than the mean strength of concrete.<sup>22</sup> Consequently, the overall safety factor, defined as the mean of test data divided by the design load, is for shear failures of smaller concrete structures about 3.5 to 8. This excessive safety factor is what has made it possible to ignore the size effect in design codes.<sup>22</sup> Not with total success, though—aside from lapses in quality control and detailing, the size effect was doubtless a major contributing factor in most shear failures of large concrete structures.

### RESEARCH SIGNIFICANCE

The significance of introducing the size effect is that the failure risk for large structures would get diminished. Additionally, the load capacity predicted by the code equation for smaller structures could be set higher, which would improve design economy and allow slenderer, aesthetically pleasing, and more efficient designs.

### PUNCHING SHEAR IN CURRENT DESIGN CODES

For the punching load capacity  $V_c$  due to concrete, the current standard ACI 318 specifies the formulas<sup>23</sup>

$$V_c = \lambda b_o d \sqrt{f_c} \text{ for no shear reinforcement} \quad (2)$$

$$V_u = \lambda b_o d \sqrt{f_c} + A_{sw} f_{yw} \frac{d}{s_w} \text{ with shear reinforcement} \quad (3)$$

where  $f_c$  is in psi;  $d$  is in inches;  $A_{sw}$  is cross-sectional area of one shear reinforcement layer around the column;  $f_{yw}$  is yield strength of shear reinforcement;  $\lambda = 4$  for U.S. customary units (or 1/3 for SI units) for no shear reinforcement, 3 (or 1/4, respectively) if reinforced by studs, and 2 (or 1/6) if by stirrups; and  $s_w$  is distance between shear reinforcement layers, measured in radial direction.

Eurocode 2 (2004)<sup>24</sup> specifies

$$V_c = \lambda \xi (100 \rho f_c)^{1/3} b_{oE} d \text{ for no shear reinforcement} \quad (4)$$

$$V_u = 0.75 \lambda \xi (100 \rho f_c)^{1/3} b_{oE} d + A_{sw} \sigma_{sw} 1.5 \frac{d}{s_w} \text{ with shear reinforcement} \quad (5)$$

$$\xi = 1 + \sqrt{\frac{200 \text{ mm}}{d}} \leq 2.0; \sigma_{sw} = 1.15(250 + 0.25d) \leq f_{yw} \quad (6)$$

where  $\rho$  is flexural reinforcement ratio, calculated for two-way slabs as the geometric average of reinforcement ratios for each direction—that is,  $\rho = \sqrt{\rho_x \rho_y}$  and  $\lambda = 5$  (or 0.18 for SI units), considered to have the dimension of  $(\text{MPa})^{2/3}$  if  $f_c$  is in MPa.

The Model Code 2010 of  $fib^{25}$  specifies the formula

$$V_c = k_\psi \sqrt{f_c} b_o d \text{ for no shear reinforcement} \quad (7)$$

$$V_u = k_\psi \sqrt{f_c} b_o d + \sum A_{sm} \sigma_{sw} \text{ with shear reinforcement} \quad (8)$$

where  $\sigma_{sw} (\leq f_{yw}) = \frac{E_s \Psi}{6} \left( 1 + \frac{f_b}{f_{yw}} \frac{d}{\phi_w} \right)$  is stress in shear reinforcement and

$$k_\psi = \min \left( 0.6, \frac{1}{1.5 + 0.9 k_{dg} \Psi d} \right) \quad (9)$$

where  $k_\psi$  has the dimension of  $\text{MPa}^{1/2}$  if  $f_c$  is in MPa;  $d_g$  is maximum aggregate size, in mm;  $k_{dg} (\geq 0.75) = 32/(d_g + 16 \text{ mm})$ ; and  $\Psi$  is the slab rotation defined in CSCT<sup>26</sup> for different cases. For the first level of approximation (LoA),  $\Psi = 1.5(r_s/d)(f_{yd}/E_s)(m_s/m_R)^{1.5}$ , wherein  $r_s$  is the distance to zero radial moment, recommended as 22% of slab span;  $m_s$  is the design moment in support strip, which can be taken as  $(V_d/8)$ ;  $V_d$  is design shear force; and  $m_R$  is the nominal moment capacity per unit width in support strip. There are four levels of approximations for the slab rotation  $\Psi$ ; the simplest one (LoA I), used herein, is  $m_s = m_R$ . The accuracy of the MC 2010 provision depends, of course, on the accuracy of the rotation calculations.

These three code formulas are compared in Fig. 1(a) to 1(c) (for the no shear reinforcement case) with the raw (unfiltered) ACI 445-C database, where the measured  $v_c$ , divided by  $f_c^{1/2}$  for ACI and Model Code, and by  $f_c^{1/3}$  for Eurocode, are plotted versus  $d$  in logarithmic scales. For ACI 318, the formulas give a horizontal line; that is, there is no size effect. For Eurocode 2004, the size effect term  $\xi$  in Eq. (6) approaches a horizontal asymptotic slope for  $d \rightarrow \infty$ . For Model Code 2010, there is size effect given by factor  $k_\psi$  in Eq. (7), which has, for  $d \rightarrow \infty$ , an asymptote proportional to  $d^{-1}$ —that is, an asymptote of slope  $-1$  in a log-log plot. Figure 1(d) shows the size effect proposed herein, discussed later.

In plotting these size effect curves, all the parameters other than  $d$  had to be fixed. They were fixed at values equal to the average values in the database. Because of the huge scatter, it is impossible to decide, from comparison to the data cloud alone, which size effect equation is better. The huge scatter is caused not only by the random differences among different concretes, labs, countries, and objectives of the experimenters, but also, and largely, by the fact that the means of secondary variables (such as  $\rho$ ,  $b/d$ ...) in subsequent size intervals are not uniform, varying greatly with  $d$ . Hence, the plots in Fig. 1 are not size effect plots. So, how does one obtain meaningful size effect plots?

## DATABASE AND ITS FILTERING TO REMOVE BIAS IN SECONDARY VARIABLES

Figure 2, Column 1 (c.1), Row I (r.I), shows the entire database of 440 measured values of the nominal punching shear strength  $v_c$  of reinforced concrete slabs with no shear reinforcement;  $v_c$  is plotted as a function of the effective slab depth  $d$ .

To obtain a large database, concrete researchers must collect, from many sources, data that have not been obtained according to a systematic sampling scheme. This inevitably makes the database statistically biased. One source of bias is that the test data for small sizes are much more numerous than for large sizes. This makes the database heteroscedastic. It can be mitigated by introducing weights inversely proportional to data density. Using  $\log d$  (rather than  $d$ ) as the coordinate also helps.

Another source of bias, a major one, is a simultaneous variation of the means of dimensionless characteristics, such as  $\rho$  and  $b/d$ , throughout subsequent size intervals as the slab size increases. This kind of bias is inevitable when the testing cannot be centrally coordinated according to a proper statistical sampling scheme. It plagues all concrete databases collected from many labs worldwide.

Both sources of bias can, in theory, be overcome by nonlinear weighted multivariate regression, which will be presented later. However, for the regression to be fully effective, the mathematical form of the dependence of the secondary variables such as  $\rho$  or  $b/d$  must be reasonably well known or deduced in advance. Unfortunately, this is not true for some variables, and especially for the effect of different concrete compositions. It is, therefore, useful to first clarify the basic size effect trend purely statistically by filtering the database, as described next.

To reduce the number of variables, the authors exploited the usual assumption that the shear strength is roughly proportional to  $f_c^{1/2}$ . So we study the variation of  $v_c f_c^{1/2}$ . The size range is subdivided into several intervals of constant width in  $\log d$  (five in Fig. 2). The averages of secondary influencing variables such as steel ratio  $\rho$  and ratios  $b/d$  and  $c/b$ , calculated separately for each size interval, should ideally be nearly the same for all the size intervals. However, as seen in the Rows III, IV, and V of c.1 in Fig. 2, the averages of  $\rho$ ,  $b/d$ , and  $c/b$  vary significantly through the subsequent size intervals. The interval average of  $\rho$  decreases with increasing size even by an order of magnitude and the interval average of  $b/d$  decreases more than three times. Thus, the database plot as function of  $d$  does not show size effect. Rather, it shows a mixture of the effects of  $d$ ,  $\rho$ ,  $b/d$ , and  $c/b$ . Also note in Fig. 2, c.1, r.II, that the interval averages of normalized shear strength for the entire database (shown by solid diamond points) are highly scattered and do not show a clear trend.

In previous works on beam shear,<sup>27,28</sup> a filtering program was developed and refined to delete, one-by-one, in an unbiased way (without human intervention), the upper and lower outlier points from each size interval, to produce a data subset with nearly uniform values of the interval means of the secondary parameters—that is, a subset minimizing the variance of the means of the secondary variables (such as  $\rho$ ,  $b/d$ , ...) in the individual size intervals.

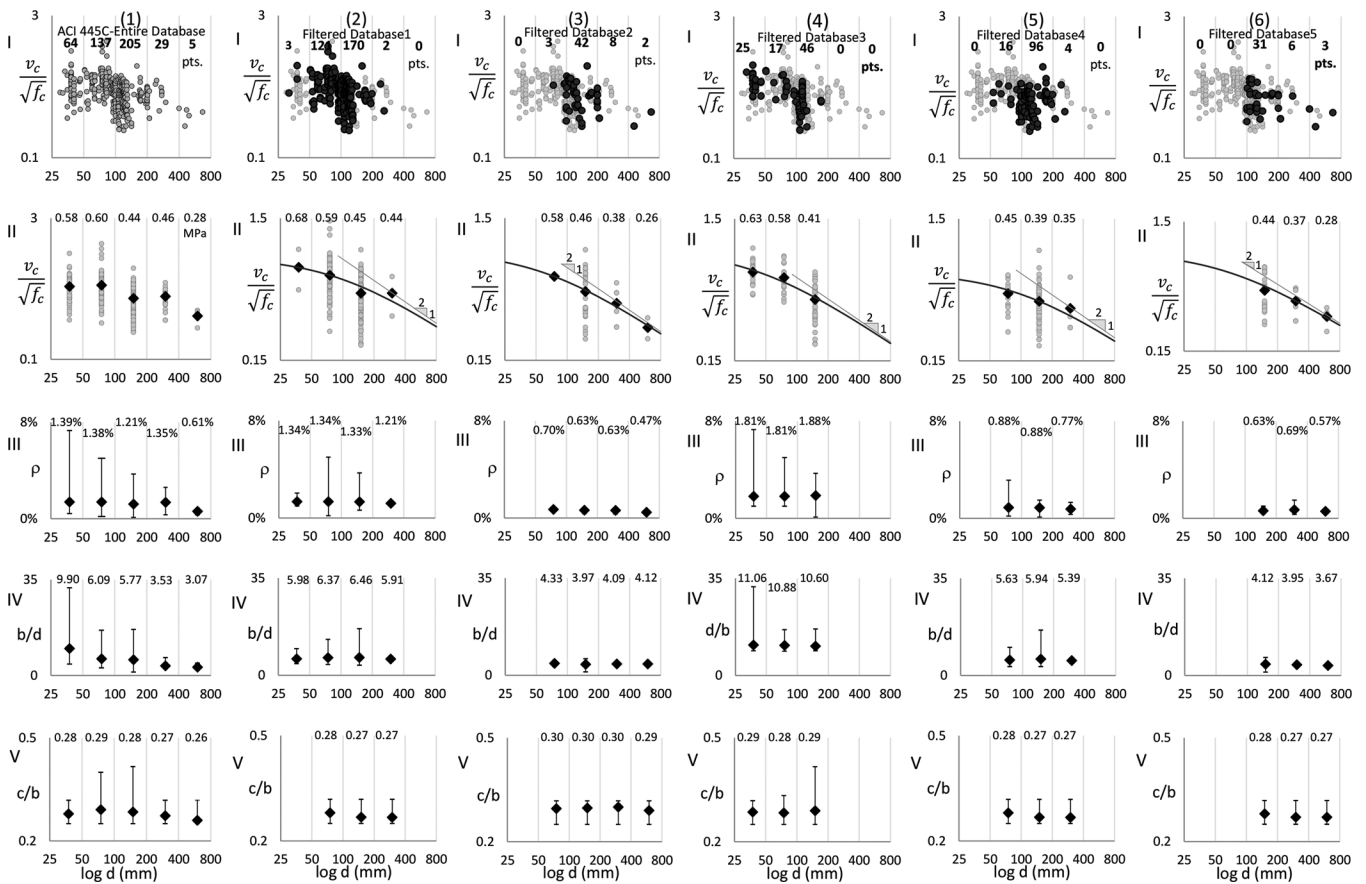


Fig. 2—Column 1: Entire database; Columns 2 to 6: filtered database and mean values of flexural reinforcement ratio  $\rho$ , aspect ratio  $b/d$ , shape factor  $c/b$  and their variations inside size intervals;  $v_c$  versus  $d$  plots are in log scale ( $\times 12$  for  $\rho$  in Rows I and II).

To be specific, denote by  $Y_{kj}$  ( $j = 1, 2, \dots, N_k$ ) all the individual data points in size interval number  $k$  ( $k = 1, 2, \dots, N_{int}$ ) (herein,  $Y_{kj}$  are the  $v_c$  values). The computer program produces data subsets by deleting database points  $Y_{kj}$  one by one. Each point to be deleted is chosen (by the computer) such that its deletion would meet one of the following two objectives: 1) the greatest possible reduction of the sum of squared deviations of the size interval means of the secondary variables from certain chosen values; or 2) the greatest possible reduction of the variance of the size interval means of the secondary variables.

Only Objective 1 is pursued herein. The minimization is applied simultaneously to all important secondary variables—that is, to the overall combined variance for Objective 1 (or to the combined sum of squared deviations for Objective 2). The deletions terminate when the coefficient of variation of the interval means attains a specified small enough value, such as 5%.

Filtering with Objective 1 generally leads to deletion of fewer data than Objective 2. However, the fact that many outliers have to be deleted may be seen as statistically objectionable. This objection can be avoided by running several different filtering runs with Objective 1. In one filtering run, a relatively high value of parameter  $\rho$  may be chosen as the desired average of  $\rho$  for all the intervals. In that case, none of the outliers on the high side gets deleted but many do on the low side. In another filtering run, a relatively low value of parameter  $\rho$  may be chosen as the desired average of

secondary variables for all the intervals. In that case, none of the outliers on the low side of the distribution of  $\rho$  values gets deleted but many do on the high side. In this way, almost every point of the database may be included in at least one of the filtered data subsets produced. In other words, none, or almost none, of data point gets completely ignored.

The resulting interval averages for  $\rho$ ,  $b/d$ , and  $c/b$ , obtained using Objective 1, are shown by the solid diamond points in Rows III, IV, V of c.2-6 of Fig. 2. As seen from the solid diamond points in Rows II of all these columns, a clearer size effect trend has now emerged (the smooth curves show the optimum least-square fits of the solid diamond points by the size effect law discussed later). For comparison, the complete database of 440 points is shown in Fig. 2 c.1, r.I. This database is repeated in c.2-6 of Fig. 2, r.I, in which the points that remain after filtering in each case are shown by black circles and the deleted ones by gray circles.

As seen, the filtering (with Objective 1) leads to a clear size effect trend (and so would the filtering with Objective 2).

There are some drawbacks, too. The main drawback is that when the mean of interval averages of a secondary variable is selected to lie too close to the upper or lower margin of the scatter-band, the filtered database may lose too many points from the original database, making the filtered data subset much too small. This drawback could be diminished only by a larger database. Another drawback is that most of the slab sizes  $d$  in the filtered database may be below the typical

sizes in practical use. Both these drawbacks are mitigated by weighted multivariate regression analysis, discussed next.

### PROPOSED SHEAR-STRENGTH EQUATION

Based on the previous experience reviewed in Reference 21 and on the energetic size effect law that was shown to be generally applicable to quasibrittle failures and was endorsed by ACI Committee 446,<sup>29</sup> the following equation is proposed

$$V_u = V_c + V_s, \quad V_c = b_o d v_c \quad (10)$$

$$v_c = v_o \theta, \quad v_o = \lambda \sqrt{f_c} (100\rho)^{0.3} \left(\frac{d}{b}\right)^{0.2} \left(\frac{c}{b}\right)^{0.4} \quad (11)$$

$$\theta = \frac{1}{\sqrt{1+d/d_o}} \quad (12)$$

$$V_s = 0.9 A_{sw} f_{yw} \left(\frac{d}{s_w}\right) \left(\frac{c}{b}\right)^{0.3} \quad (13)$$

where  $v_o$  is value of  $v_c$  for vanishing size  $d$ ;  $\theta$  is size effect factor<sup>30-32</sup> unanimously endorsed for shear failures by ACI Committee 446<sup>29</sup>;  $d_o$  is transitional size (empirical, 60 mm [2.36 in.] according to database regression);  $V_u$  is punching shear load;  $V_s$  is punching load capacity due to shear reinforcement;  $\lambda$  is empirical constant = 2.0 MPa<sup>1/2</sup> in SI (or 24.1 psi<sup>1/2</sup> in U.S. customary units). The exponent values 0.3, 0.2 and 0.4 of  $\rho$ ,  $d/b$ , and  $c/b$  were obtained by least-square optimization of the fit of entire database, as described later.

### CRITICAL SIZE EFFECT COMPARISON WITH MODEL CODE 2010 AND EUROCODE 2004

The size dependence of shear strength according to Eurocode 2004 and Model Code 2010 (Fig. 1(b) and 1(c)) is invalidated by the trend of the interval means in Fig. 2 r.II, c.1-6, at all. In Fig. 2, there is no hint of a slope steeper than  $-1/2$ , and certainly no slope approaching  $-1$ , as implied by Model Code 2010. Furthermore, the asymptotic slopes of 0 and  $-1$  implied by the Eurocode and Model Code size effect (Fig. 1(b) and 1(c)), as well as by the previous Swiss design code, violate the energy balance (or fracture mechanics) because the energy released from the structure by a crack increment does not match the energy dissipated by that increment at fracture front.<sup>31,32</sup> The steepest possible slope is  $-1/2$ , corresponding to energy dissipation by a pointwise crack tip (which is an acceptable approximation only for very large sizes). If the dissipation occurs in a wider and longer fracture process zone, the slope is milder than  $-1/2$ , and if the dissipation is distributed widely, the slope is 0 (no size effect).

Note also that if  $v_c$  is increased in proportion to  $1/d$  (as in Model Code), the shear force  $V_c = b_o d v_c$  is independent of  $d$ . Thus,  $V_c$  approaches, for large  $d$ , a finite bound (that is, a horizontal asymptote). This feature defies common sense—it means that, for example, the doubling of thickness of a slab

whose thickness is already near the asymptotic bound would cause no further increase of the punching force capacity  $V_c$ .

To understand why the impossible asymptotic slope of  $-1$  is exhibited by MC2010 (with LoA1), note that, to ensure geometric similarity in size effect analysis, all the spatial dimensions must be scaled in proportion while all the dimensionless parameters are kept constant. However, in LoA 2 or 3 of Model Code 2010, the dimensionless ratio of acting moment  $m_s$  to moment capacity  $m_R$ , is varied with size ( $m_s \approx$  function of  $V_u$ ). This leads to an apparent asymptotic size effect slope that combines the effect of the size  $d$  with the effect of variable (dimensionless) rotation  $\psi$  (or strain). This is not size effect. It is a deceptive curve of apparent size effect distorted by simultaneous variation of a dimensionless variable, the strain.

In general, the strain cannot be used to characterize fracture-induced failures, for which the balance of released and dissipated energy (or the first law) is the basic principle. By imagining a convenient variation of some secondary dimensionless parameters, one could get any desired (and misleading) dependence of structure strength on  $d$ . Besides, unlike the size effect curve, the validity of such imagined curves of structure strength versus size, as in LoA 2 or 3, cannot be verified by any elementary principles such as energy conservation.

### VERIFICATION AND CALIBRATION BY WEIGHTED MULTIVARIATE REGRESSION FOR SLABS WITHOUT SHEAR REINFORCEMENT

Most of the data sets in the literature contain only a single slab depth or a negligible range of depths. Deleting from the database the test series in which the slab depth was a variable with non-negligible range eliminates 95% of all test data, and even most of the remaining data are not geometrically scaled, as required for separating the size effect from other effects. Similar to shear failure of beams,<sup>28,33,34</sup> this is why a filtered analysis of the database is needed to reveal trends, and why a theoretical support in quasibrittle fracture mechanics is indispensable.

The maximum load in punching shear is reached only after stable growth of a large crack, and the location of the crack tip at maximum load is determined by mechanics. The volume of concrete zone in which mechanics permits the crack tip to be located is much too small compared to the volume of structure. It consists of only a few representative volume elements (RVEs) of concrete and, thus, many locations with random strength cannot get sampled by the potential crack front. Therefore, the size effect on the mean strength cannot be statistical. Rather, it must be energetic—that is, deterministic—and must follow the size effect law of quasibrittle fracture mechanics<sup>30-32</sup> as expressed by the size effect factor  $\theta$  in Eq. (12). The analytical form of this factor is herein supported by the fits of mean trends of the filtered subsets of database; refer to the solid curves in Fig. 2, r.II, c.2-6.

The filtered database subsets cannot be used for statistics of errors because many data had to be deleted. To this end, the entire database must be used, which requires least-square fitting by a shear strength formula using multivariate regression. In this regression, the data in each of the five size intervals are assigned weights inversely proportional to the

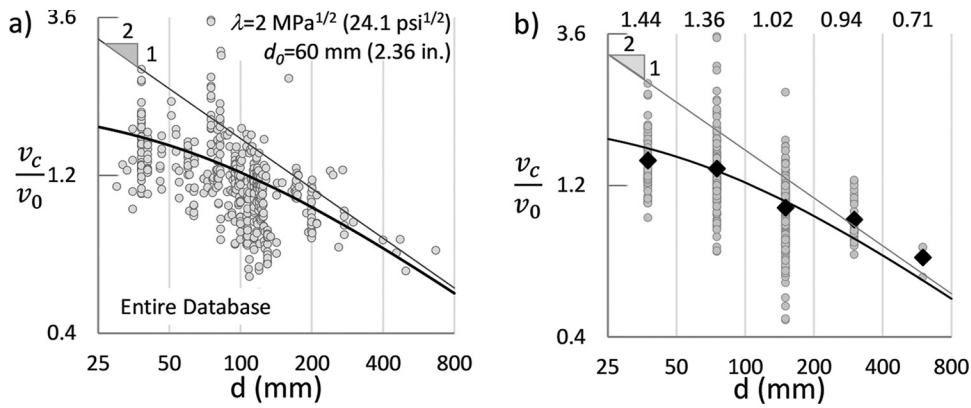


Fig. 3—(a) Illustration of size effect fit on entire database, normalized by secondary variables (excluding  $\lambda$  in Eq. (11)) found by multivariate regression; and (b) size effect fit for normalized mean strengths of subdivided data into size intervals. (Note: 1 mm = 0.0394 in.)

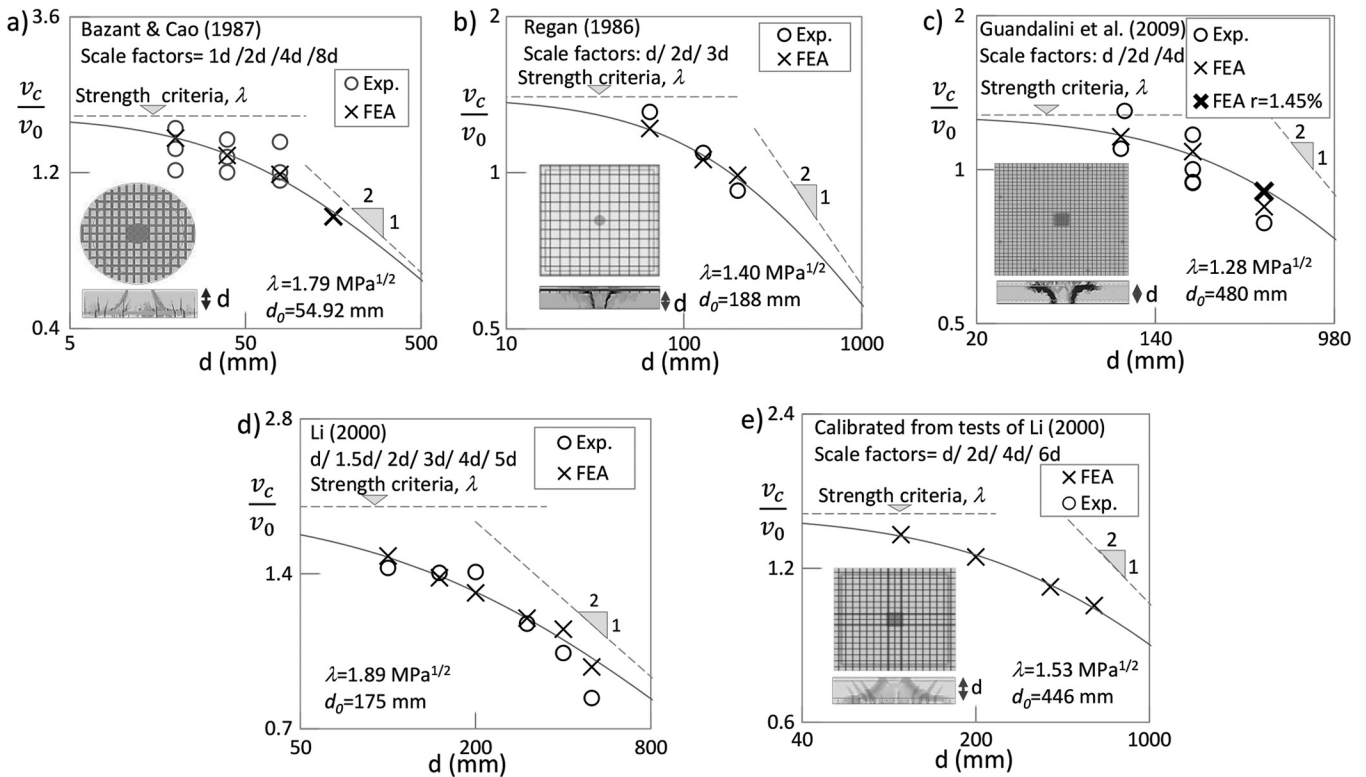


Fig. 4—Size effect analysis of experiments of: (a) Bazant and Cao<sup>1</sup>; (b) Regan<sup>7</sup>; (c) Guandalini et al.<sup>9</sup> and created specimen with 1.45% reinforcement ratio for size effect analysis; (d) Li<sup>40</sup>; and (e) created FE specimens from calibrated data of Li, and sample of corresponding fracture patterns from FEA on left bottoms. (Note: 1 MPa = 145 psi; 1 mm = 0.0394 in.;  $\lambda$  is excluded from  $v_o$ .)

number of data in each interval. Such weighting suppresses the bias due to crowding of many data at small sizes  $d$  and scarcity of data at large sizes  $d$  (for details and further justification, refer to similar weighted optimization for beam shear in References 27, 33, and 34).

The results of the weighted regression of the entire database are shown in Fig. 3(a), in which the database points represent the values of normalized shear strength  $v_c$  divided by  $v_o$ , where  $v_c$  are the measured punching strength values and  $v_o$  are the values from the optimized fit by Eq. (11) with excluding the parameter  $\lambda$ . This is another way to eliminate the effect of variation of secondary variables with  $d$ , but, of course, it meets success only if a realistic form of the formula, with a low coefficient of variation of errors, is

found. Figure 3(b) (in which the solid diamond points show the interval averages) shows that the ACI 446 size effect factor  $\theta$  (solid curve) matches the data trend well.<sup>29</sup> The transition to asymptotic slope,  $-1/2$ , was for shear failures verified also by Ruiz et al.,<sup>4</sup> and was supported by a different type of analysis.

#### MICROPLANE FINITE ELEMENT ANALYSIS OF TEST SERIES WITH DIFFERENT SLAB SIZES

There exist a few punching test series where the size was varied significantly (Fig. 4(a) to 4(e)). The data from each of these test series have been optimally fitted by a finite element (FE) program with a realistic damage constitutive law. In this program, the constitutive law was the microplane model

M7<sup>35</sup> (which is the latest and most realistic in a series of microplane models for concrete developed at Northwestern University). The constitutive material properties are characterized by a relation between the stress and strain components (or forces and displacements) on the microlevel<sup>36</sup> (or, more precisely, the mesolevel). The stress-strain relations are defined not in terms of the macrolevel continuum tensors, but in terms of the stress and strain vectors on planes of all possible orientations within the material, which are called the microplanes.

Based on the microplane constitutive law, the stress vector is, on each microplane, calculated from the strain vector obtained as the microplane projection of the macrolevel continuum strain tensor (this is called the kinematic constraint). The stress tensor is calculated from the stress vectors on all the microplanes by means of the principle of virtual work. The latest version of microplane models, M7, which uses an explicit numerical algorithm, was shown capable of realistically predicting the quasibrittle material damage behaviors over a broad range of loading scenarios.<sup>35,37</sup> Model M7 is robust, always convergent, and has successfully been used in dynamic problems with greater than  $3 \times 10^7$  unknowns.

All the simulations herein are conducted with commercial software ABAQUS, in which model M7 is introduced in VUMAT as a user's material subroutine. To avoid spurious mesh sensitivity, the crack band model is used as the localization limiter.<sup>38</sup> To avoid some loss in accuracy due to scaling of the postpeak,<sup>39</sup> a constant element size  $h_c$  (equal approximately to double the maximum aggregate size) is used in all the present computations. Linear hexahedral or tetrahedral elements are chosen. The adjustable parameters of M7 sufficed to match the main material properties.

After calibration by fitting of the available punching test data of each test series, model M7 was used to calculate the values of  $v_d/v_o$  for various sizes. Compared to the highly scattered individual test data shown by circles in Fig. 4, the calibrated FE results, shown by the x-points in the figures, have the advantage of no scatter. One such series<sup>1</sup> reported tests of geometrically scaled circular slabs of three different sizes in the ratio 1:2:4; refer to Fig. 4(a) (because of the use of reduced maximum aggregate size of 4.7 mm [0.18 in.], these tests were not included in the ACI 445-C database). The depth  $d$  of the smallest slab was 20 mm (0.79 in.). The calibrated model is then used to calculate the x-point for each test size and an extra point for double the size of the largest slab tested. The x-points agree well with the solid curve of the ACI 446 size effect factor,<sup>29</sup> Eq. (12).

Similar tests of rectangular slabs with circular columns, of size ratio 1:2:3, were carried out by Regan<sup>7</sup>; refer to Fig. 4(b). The aspect ratio  $b/d$  is constant for all slabs, although the flexural reinforcement ratio varies slightly. The maximum aggregate size was 20 mm (0.79 in.) for the specimens modeled herein (tests with reduced aggregate sizes in the smaller and medium specimens were also conducted but are not used here).

Recently, punching shear tests with thicknesses in the ratio 1:2:4 were conducted by Guandalini et al.,<sup>9</sup> with  $d = 0.5$  m (19.7 in.) for the largest slab. The slabs were geometrically

scaled except that the reinforcement ratios varied slightly, which was taken into account in FE analysis. Even though modest nonuniformity of the reinforcement ratios slightly taints the size effect regression, the fit for a uniform reinforcement ratio of 1.45% gives the mean trend (Fig. 4(c)).

Figure 4(d) shows the size effect of the experiments by Li,<sup>40</sup> who tested six square slabs with a slight variation in flexural reinforcement ratio, punched by square columns with different aspect ratios. Normalizing the measured maximum loads and the corresponding loads from FE simulations indicates a strong size effect trend for larger sizes. The test result for the smallest size is overestimated, as shown in Fig. 4(d). After the FE code with microplane model is calibrated by fitting Li's experiments, the code is used to simulate the size effect. The simulations show excellent agreement with the ACI 446 size effect,<sup>29</sup> Eq. (12) (solid curve in Fig. 4(e)).

Overall, Fig. 4(a) to 4(e) demonstrate a significant transitional size effect on the punching shear strength, agreeing with the size effect law and with FE simulations based on microplane model M7.

### MICROPLANE FINITE ELEMENT ANALYSIS OF TEST SERIES WITH SHEAR REINFORCEMENT

Although the shear reinforcement of slabs does not enhance ductility, it changes the cracking pattern and significantly elevates the load and deformation capacity because it intersects, and thus suppresses, the conical fracture produced by the punching load from the column. There is a variety of transverse reinforcement types, such as stirrups, studs and assorted profiles, and a variety of reinforcement layouts around the column. This increases uncertainties in predicting the punching load capacity.

As in shear of beams, the contribution of concrete and the contribution of steel reinforcement, calculated under the assumption of yielding, are considered additive<sup>12</sup> (Eq. (3)). However, it is not guaranteed and is, in fact, doubtful for thick slabs that the steel would actually be yielding at maximum load rather than later in postpeak softening. Moreover, the failure of shear reinforcement can take different forms, such as the punch failure outside the shear reinforced area, delamination, and concrete crushing. Investigation of these diverse forms and their effects on the size effect curve is out of the scope of this study.

Unfortunately, there are no tests clearly demonstrating the size effect for slabs with shear reinforcement. Lips et al.<sup>10</sup> and Birkle<sup>41</sup> tested slabs with and without shear reinforcement, but the size range was too narrow compared to inevitable scatter. In Birkle's tests of octagonal slabs on square columns, slabs in the size ratio 1:1.53:2.09 were tested, but this range was not sufficiently broad. To reveal the size effect, the shear reinforcement ratio, which is defined as  $\rho_s = A_{sw}/(bs_w)$ , should be constant, but in these and other tests, it varied with  $d$ , as did the aspect ratio and even the concrete strength.

Figures 5(a) to 5(c) shows fitting of Birkle's tests for calibration of the microplane FE program (close fitting of the initial elastic slopes spoiled a close match of the rising curves). The size effect is then predicted with the calibrated program. As shown in Fig. 5(d), the effect of studs is to

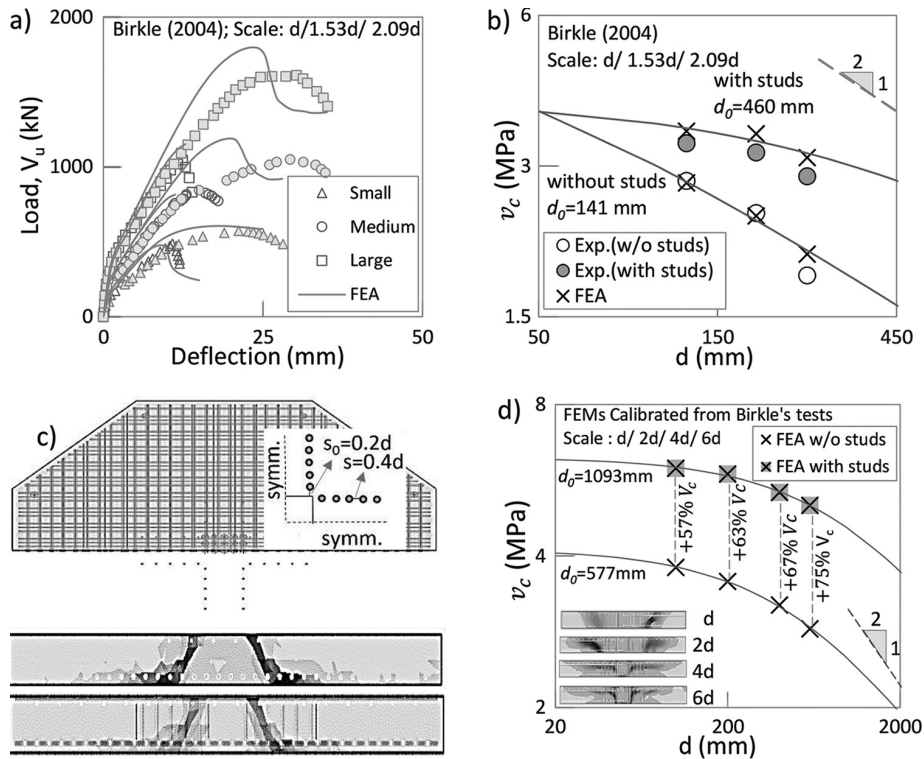


Fig. 5—(a) Experimental and corresponding FEA results of calibration from tests of Birkle<sup>41</sup>; (b) strength-versus-size plots in log-log scale; (c) sample of cracking pattern obtained from numerical simulations; and (d) size effect regression curves obtained from calibrated FE models (with and without studs). (Note: 1 MPa = 145 psi; 1 kN = 224.8 lbf; 1 mm = 0.0394 in.)

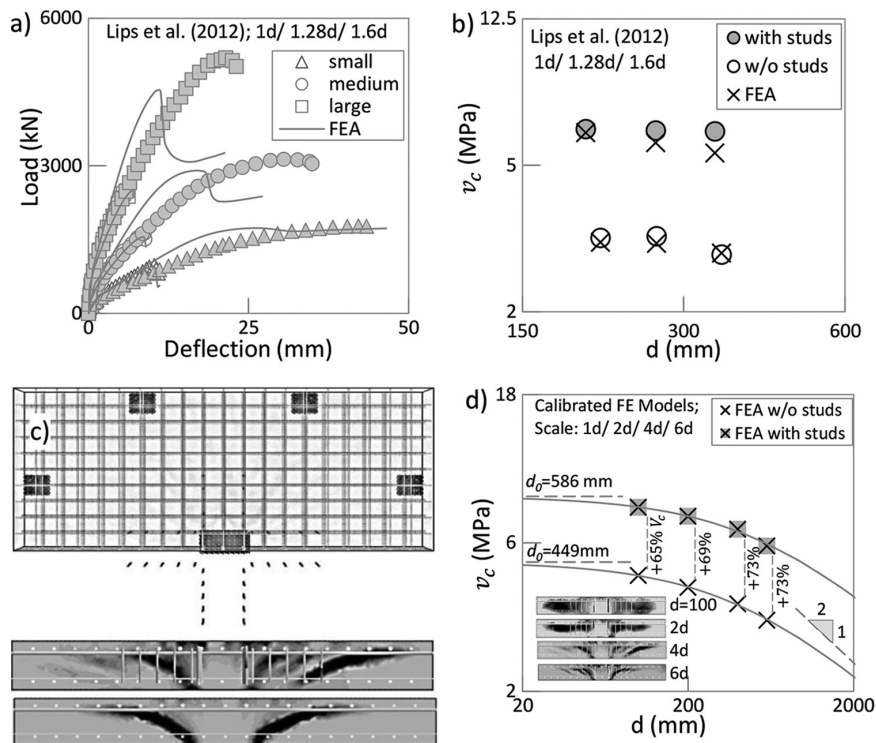


Fig. 6—(a) Experimental and corresponding FEA results of calibration from tests of Lips et al.<sup>10</sup>; (b) strength-versus-size plots in log-log scale; (c) sample of cracking pattern obtained from numerical simulations; (d) size effect regression curves obtained from calibrated FE models (with and without studs). (Note: 1 MPa = 145 psi; 1 kN = 224.8 lbf; 1 mm = 0.0394 in.)

shift the size effect curve upward. Note also that the studs, with the ACI-type layout (Fig. 5(c)), greatly increase the punching capacity.

Another demonstration of size effect can be based on Lips et al.'s<sup>10</sup> tests of square slabs with square columns (Fig. 6(a) to 6(d)). The size ratio is 1:1.28:1.6, which is again insufficient to reveal size effect directly. Calibration by data fitting



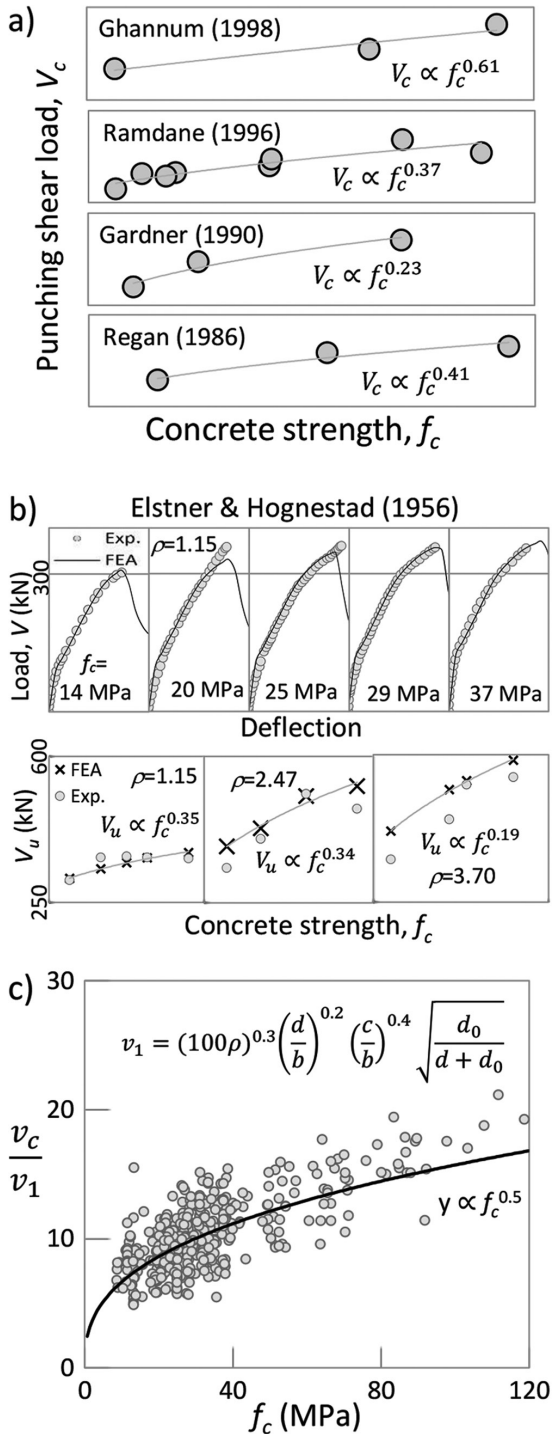


Fig. 7—(a) Illustration of concrete strength effect on punching shear capacity from tests of References 5 to 8; (b) experimental and numerical illustration of concrete strength dependency from tests of Elstner and Hognestad<sup>3</sup>; and (c) results of multivariate regression for  $f_c$ , with using entire database fit. (Note: 1 MPa = 145 psi; 1 kN = 224.8 lbf.)

with the microplane FE program, in which the initial elastic slopes were matched closely, appears in Fig. 6(a) and 6(b). Prediction of the size effect, along with the cracking pattern at maximum load, is then shown in Fig. 6(c) and 6(d). The conclusions about size effect are the same as for Birkle's tests. The simulations further demonstrate that the circular

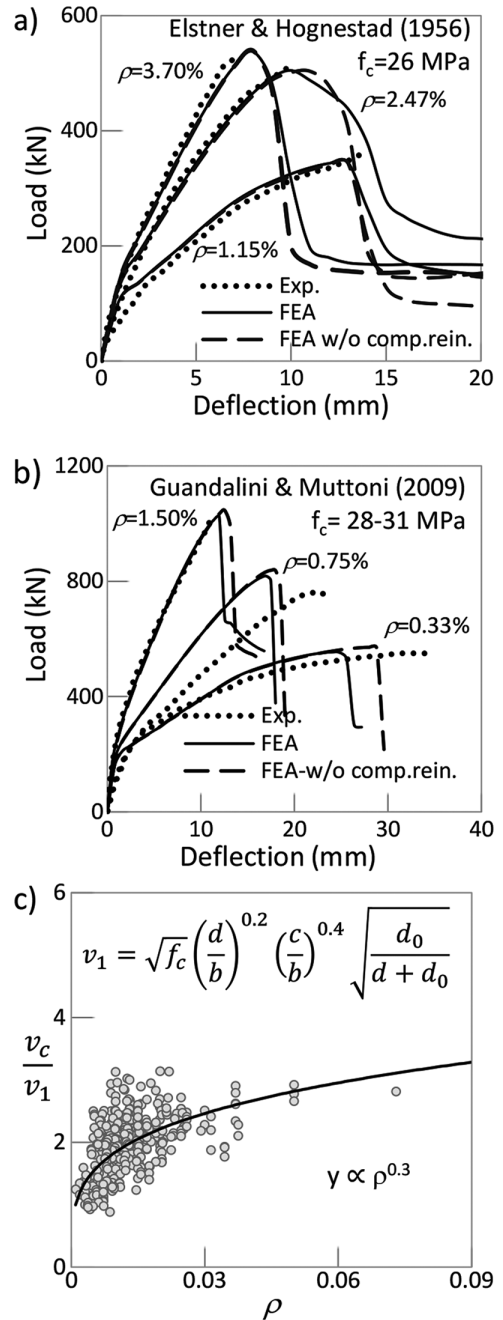


Fig. 8—Load-deflection curves of punching shear specimens with varying reinforcement ratios and corresponding FEA results from the tests of: (a) Elstner and Hognestad<sup>3</sup> and (b) Guandalini and Muttoni,<sup>9</sup> respectively; and (c) results of multivariate regression for reinforcement ratio. (Note: 1 kN = 224.8 lbf; 1 MPa = 145 psi; 1 mm = 0.0394 in.)

layout of studs provides a lesser enhancement of punching strength than does the rectangular (ACI-type) layout.

#### VERIFICATION OF OTHER TRENDS BY MICROPLANE FINITE ELEMENTS ANALYSIS

Further statistics and trends of punching shear strength of slabs with shear reinforcement can be inferred from the data in the literature,<sup>14-20,42</sup> although hardly anything more about the size effect can be concluded from these studies. The fact that  $v_c$  is approximately proportional to  $f_c^{0.5}$ ,  $\rho^{0.3}$ ,  $(d/b)^{0.2}$ , and

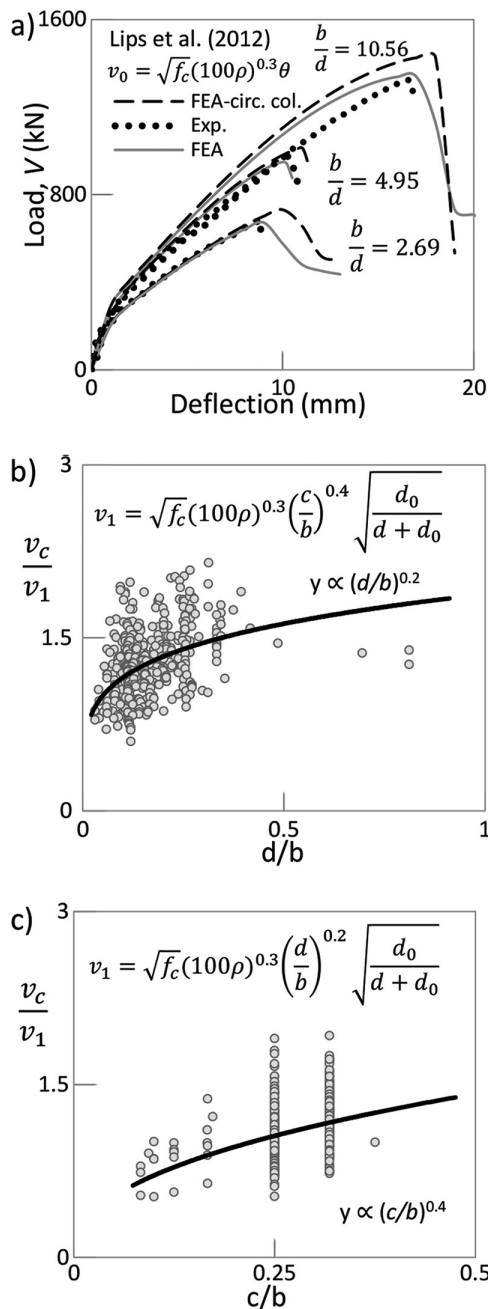


Fig. 9—(a) Illustration of aspect ratio  $b/d$  and shape effect (right bottom),  $c/b$  on load-deflection plots and corresponding FEA for square and equivalent circular columns with calibration according to tests of Lips et al.<sup>10</sup> Multivariate regression curves for (b) ratio  $d/b$ ; and (c) shape effect  $c/b$  with using entire database. (Note: 1 kN = 224.8 lbf; 1 mm = 0.0394 in.)

$(c/b)^{0.4}$  is verified by Fig. 7(c), 8(c), 9(b), and 9(c), in which the curves were calculated from the parameters obtained by weighted multivariate regression. The  $v_c$  values are in these figures normalized by the  $v_1$  values that account for the effect of other nonconstant variables (refer to the captions). This correction is applied to each data point, because the parameters in  $v_1$  are different for each. Figures 7, 8, and 9 also show calibrations and validations of the microplane FE model by load-deflection curves reported in References

3 and 5 through 10 and by comparisons with selected data from these experimenters on the effects of  $f_c^{0.5}$ ,  $\rho^{0.3}$ ,  $(d/b)^{0.2}$ , and  $(c/b)^{0.4}$ .

## CONCLUSIONS

Based on this study, the following conclusions can be made:

1. Although properly scaled tests of punching shear strength are lacking, the existing ACI 445-C database reveals a clear size effect trend after creating filtered data subsets in which the averages of secondary variables in subsequent size intervals (that is, of the steel ratio and slab thickness-to-column width ratios) are almost constant through all the intervals.

2. The data trend revealed by such filtering shows a significant size effect on the nominal punching shear strength  $v_c$  of concrete. This trend demonstrates that: a) there is no indication of a sudden slope change on the size effect curve (unlike Eurocode 2004); b) the average slope of the data trend of  $\log v_c$  versus  $\log d$  is milder, though not much milder, than  $-1/2$ ; c) there is no hint of a slope approaching  $-1$ , not even steeper than  $-1/2$ ; and d) the data are compatible with the energetic (non-statistical) size effect law.

3. The least-square multivariate regression of the complete ACI 445-C database, with weights countering uneven data distribution, indicates that the proposed formula with the ACI 446 size effect factor  $\theta$  gives a relatively good fit.

4. Although the effects of geometry ( $b/d$ ,  $c/b$ ) and of the longitudinal and shear reinforcement ratios had to be included in the optimization, simultaneous data filtering with respect to these parameters is beyond the scope of this work. Nevertheless, the size effect factor  $\theta$  obtained and validated herein can be applied to any good formula for these effects, including a formula based on plastic limit analysis, provided it fits well the small-scale test data (for which  $\theta \approx 1$ ).

## NOTE ON STRUCTURAL SAFETY

Although proper capacity reduction (or ‘understrength’) factors must be applied to the design equations, the design codes provide additional safety by scaling down the design equations to the lower margin of the data cloud. In this approach, the value of  $v_c$  given by Eq. (11) must be scaled down by the factor of 2.1. However, such an approach creates a problem for probabilistic structural analysis. If the mean prediction is not known to the analyst, such analysis becomes meaningless.

For the most up-to-date analysis of structural safety, as well as statistical and energetic size effects, refer to Reference 43.

## AUTHOR BIOS

ACI member **Abdullah Dönmez** conducts research in the Faculty of Civil Engineering, Istanbul Technical University, Istanbul, Turkey, where he received his BS, MS, and PhD in civil engineering in 2006, 2009, and 2015, respectively. He is a member of Joint ACI-ASCE Committee 445, Shear and Torsion.

ACI Honorary Member **Zdeněk P. Bažant** is a McCormick Institute Professor and W.P. Murphy Professor of Civil and Mechanical Engineering and Materials Science at Northwestern University, Evanston, IL. He is a member of ACI Committee 209, Creep and Shrinkage in Concrete; and Joint ACI-ASCE Committees 445, Shear and Torsion, and 446, Fracture Mechanics of Concrete.

## ACKNOWLEDGMENTS

Partial financial support was obtained under NSF Grant CMMI-1129449 to Northwestern University. The first author thanks The Scientific and Technological Research Council of Turkey for financially supporting his predoctoral fellowship at Northwestern.

## NOTATION

$A_{sm}$	=	cross-sectional area of all shear reinforcements within area bounded by $0.35d$
$A_{sw}$	=	cross-sectional area of one shear reinforcement layer around column
$b$	=	perimeter of loaded area (column)
$b_o$	=	control perimeter, calculated at distance $d/2$ from column face
$b_{oE}$	=	control perimeter, calculated at distance $2d$ from column face
$c$	=	side length (or short edge) of square (or rectangular) column or diameter of circular column
$D$	=	characteristic size of structure
$d$	=	effective thickness of slab, calculated as $d = (d_x + d_y)/2$
$d_0$	=	material constant characterizing transitional range
$d_g$	=	maximum aggregate size, mm
$d_o$	=	transitional size which equals to materials' characteristic lengths times structure shape parameters
$d_x, d_y$	=	distances from compression face to flexural reinforcement on x- and y-directions, respectively
$E_s$	=	Young's modulus of longitudinal reinforcement steel
$f_b$	=	bond strength, which is equal to $2f_{ct}$ , where $f_{ct}$ refers to tensile strength of concrete
$f_c$	=	concrete compressive strength
$f_{yd}$	=	yield strength of flexural reinforcement
$f_{yw}$	=	yield strength of shear reinforcement
$h$	=	slab thickness
$k_{dg}$	=	factor accounting for influence of aggregate size
$l_0$	=	length of fracture process zone
$m_R$	=	nominal moment capacity per unit width in support strip
$m_s$	=	design moment in support strip and can be taken as $V_d/8$
$r_s$	=	distance to zero radial moment and can be taken as 0.22 times the slab span
$s_w$	=	distance between shear reinforcement layers
$V$	=	shear load
$V_c$	=	punching load capacity due to concrete
$V_d$	=	design shear force
$V_s$	=	punching load capacity due to shear reinforcement
$V_u$	=	punching shear load
$v_c$	=	punching shear strength of slabs without shear reinforcement
$v_o$	=	value of $v_c$ for vanishing size $d$
$v_1$	=	normalization expression stated in figures accordingly
$\varphi_w$	=	diameter of shear reinforcement
$\lambda$	=	empirical constant for convenience
$\theta$	=	size effect term in proposed equation
$\rho$	=	flexural reinforcement ratio, calculated as $(\rho_x \rho_y)^{0.5}$
$\rho_s$	=	shear reinforcement ratio
$\rho_x, \rho_y$	=	longitudinal reinforcement ratios on x- and y-directions, respectively
$\sigma_{sw}$	=	effective stress in shear reinforcement
$\xi$	=	size effect term in EC2 provision
$\psi$	=	rotation of slab

## REFERENCES

1. Bažant, Z. P., and Cao, Z., "Size Effect in Punching Shear Failure of Slabs," *ACI Structural Journal*, V. 84, No. 1, Jan.-Feb. 1987, pp. 44-53.
2. Moe, J., "Shearing Strength of Reinforced Concrete Slabs and Footings Under Concentrated Loads," *Development Department Bulletin*, No. D47, PCA, Skokie, IL, 1961.
3. Elstner, R. C., and Hognestad, E., "Shearing Strength of Reinforced Concrete Slabs," *ACI Journal Proceedings*, V. 53, No. 7, July 1957, pp. 29-58.
4. Fernández Ruiz, M.; Muttoni, A.; and Sagaseta, J., "Shear Strength of Concrete Members without Transverse Reinforcement: A Mechanical Approach to Consistently Account for Size and Strain Effects," *Engineering Structures*, V. 99, Sept., 2015, pp. 360-372. doi: 10.1016/j.engstruct.2015.05.007
5. Ghannoum, C. M., "Effect of High-Strength Concrete on the Performance of Slab-Column Specimens," Department of Civil Engineering and Applied Mechanics, McGill University, Montréal, QC, Canada, 1998, pp. 27-67.
6. Ramdane, K. E., "Punching Shear Strength of High Performance Concrete Slabs," *Proceedings of the 4th International Symposium on Utili-*

*zation of High-Strength/High-Performance Concrete*, Paris, France, V. 3, May 1996, pp. 1015-1026.

7. Regan, P. E., "Symmetric Punching of Reinforced Concrete Slabs," *Magazine of Concrete Research*, V. 38, No. 136, 1986, pp. 115-128. doi: 10.1680/mac.1986.38.136.115
8. Gardner, N. J., "Relationship of the Punching Shear Capacity of Reinforced Concrete Slabs with Concrete Strength," *ACI Structural Journal*, V. 87, No. 1, Jan.-Feb. 1990, pp. 66-71.
9. Guandalini, S.; Burdet, O.; and Muttoni, A., "Punching Tests of Slabs with Low Reinforcement Ratios," *ACI Structural Journal*, V. 106, No. 1, Jan.-Feb. 2009, pp. 87-95.
10. Lips, S.; Ruiz, M. F.; and Muttoni, A., "Experimental Investigation on Punching Strength and Deformation Capacity of Shear-Reinforced Slabs," *ACI Structural Journal*, V. 109, No. 6, Nov.-Dec. 2012, pp. 889-900.
11. Ruiz, M. F.; Mirzaei, Y.; and Muttoni, A., "Post-punching Behavior of Flat Slabs," *ACI Structural Journal*, V. 110, No. 5, Sept.-Oct. 2013, pp. 801-812.
12. Elgabry, A. A., and Ghali, A., "Design of Stud-shear Reinforcement for Slabs," *ACI Structural Journal*, V. 87, No. 3, May-June 1990, pp. 350-361.
13. Oliveira, D. R. C.; Regan, P. E.; and Melo, G. S. S. A., "Punching Resistance of RC Slabs with Rectangular Columns," *Magazine of Concrete Research*, V. 56, No. 3, 2004, pp. 123-138. doi: 10.1680/mac.2004.56.3.123
14. Ferreira, M. P.; Melo, G. S.; Regan, P. E.; and Vollum, R. L., "Punching of Reinforced Concrete Flat Slabs with Double-Headed Shear Reinforcement," *ACI Structural Journal*, V. 111, No. 2, Mar.-Apr. 2014, pp. 363-374.
15. Trautwein, L. M.; Bittencourt, T. N.; Gomes, R. B.; and Della Bella, J. C., "Punching Strength of Flat Slabs with Unbraced Shear Reinforcement," *ACI Structural Journal*, V. 108, No. 2, Mar.-Apr. 2011, pp. 197-205.
16. Heinzmann, D.; Etter, S.; Villiger, S.; and Jaeger, T., "Punching Tests on Reinforced Concrete Slabs with and without Shear Reinforcement," *ACI Structural Journal*, V. 109, No. 6, Nov.-Dec. 2012, pp. 787-794.
17. Borges, L. L. J.; Melo, G. S.; and Gomes, R. B., "Punching Shear of Reinforced Concrete Flat Plates with Openings," *ACI Structural Journal*, V. 110, No. 4, July-Aug. 2013, pp. 547-556.
18. Hegger, J.; Ricker, M.; and Sherif, A. G., "Punching Strength of Reinforced Concrete Footings," *ACI Structural Journal*, V. 106, No. 5, Sept.-Oct. 2009, pp. 706-716.
19. Vollum, R. L.; Abdel-Fattah, T.; Eder, M.; and Elghazouli, A. Y., "Design of ACI Type Punching Shear Reinforcement to Eurocode 2," *Magazine of Concrete Research*, V. 62, No. 1, 2010, pp. 3-16. doi: 10.1680/mac.2008.62.1.3
20. Gomes, R. B., and Regan, P. E., "Punching Resistance of RC Flat Slabs with Shear Reinforcement," *Journal of Structural Engineering*, ASCE, V. 125, No. 6, 1999, pp. 684-692. doi: 10.1061/(ASCE)0733-9445(1999)125:6(684)
21. Ospina, C. E., Birkle, G., and Widiyanto, "ACI 445 Punching Shear Collected Databank," *Network for Earthquake Engineering Simulation (database) Dataset*, 2011. doi: 10.4231/D3TX35618
22. Bažant, Z. P., and Yu, Q., "Reliability, Brittleness, Covert Understrength Factors, and Fringe Formulas in Concrete Design Codes," *Journal of Structural Engineering*, ASCE, V. 132, No. 1, 2006, pp. 3-12. doi: 10.1061/(ASCE)0733-9445(2006)132:1(3)
23. ACI Committee 318, "Building Code Requirements for Structural Concrete (ACI 318-11) and Commentary," American Concrete Institute, Farmington Hills, MI, 2011, 503 pp.
24. Eurocode 2, "Design of Concrete Structures Part 1: General Rules and Rules for Building. European Committee for Standardization," Brussels, Belgium, 2004, 241 pp.
25. ModelCode, 2010, "Fédération Internationale du Béton: Model Code 2010," Lausanne, Switzerland, 2010, pp. 382-393.
26. Muttoni, A., and Schwartz, J., "Behaviour of Beams and Punching in Slabs without Shear Reinforcement," *IABSE Colloquium*, V. 62, No. EPFL-CONF-111612, 1991, pp. 703-708.
27. Bažant, Z. P., and Yu, Q., "Minimizing Statistical Bias to Identify Size Effect From Beam Shear Database," *ACI Structural Journal*, V. 105, No. 6, Nov.-Dec. 2008, pp. 685-691.
28. Yu, Q.; Le, J. L.; Hubler, M. H.; Wendner, R.; Cusatis, G.; and Bažant, Z. P., "Comparison of Main Models for Size Effect on Shear Strength of Reinforced and Prestressed Concrete Beams," *Structural Concrete*, V. 17, No. 5, 2016, pp. 778-789. doi: 10.1002/suco.201500126
29. Bažant, Z. P.; Yu, Q.; Gerstle, W.; Hanson, J.; and Ju, J. W., "Justification of ACI-446 Proposal for Updating ACI Code Provisions for Shear Design of Reinforced Concrete Beams," *ACI Structural Journal*, V. 104, No. 5, Sept.-Oct. 2007, pp. 601-610. (with errata, title correction, Nov.-Dec., p. 767)
30. Bažant, Z. P., "Size Effect in Blunt Fracture: Concrete, Rock, Metal," *Journal of Engineering Mechanics*, ASCE, V. 110, No. 4, 1984, pp. 518-535. doi: 10.1061/(ASCE)0733-9399(1984)110:4(518)

31. Bažant, Z. P., and Planas, J., *Fracture and Size Effect in Concrete and Other Quasibrittle Materials*, CRC Press, Boca Raton, FL, 1998, 640 pp.
32. Bažant, Z. P., *Scaling of Structural Strength*, Hermes Penton Science (Kogan Page Science), London, UK, 2002, pp. 21-52.
33. Bažant, Z. P., and Yu, Q., "Designing Against Size Effect on Shear Strength of Reinforced Concrete Beams Without Stirrups: I. Formulation," *Journal of Structural Engineering*, ASCE, V. 131, No. 12, 2005, pp. 1877-1885. doi: 10.1061/(ASCE)0733-9445(2005)131:12(1877)
34. Bažant, Z. P., and Yu, Q., "Designing Against Size Effect on Shear Strength of Reinforced Concrete Beams Without Stirrups: II. Verification and Calibration," *Journal of Structural Engineering*, ASCE, V. 131, No. 12, Dec. 2005, pp. 1885-1897.
35. Caner, F. C., and Bažant, Z. P., "Microplane Model M7 for Plain Concrete: I. Formulation," *Journal of Engineering Mechanics*, ASCE, V. 139, No. 12, 2013, pp. 1714-1723. doi: 10.1061/(ASCE)EM.1943-7889.0000570
36. Bažant, Z. P., and Ožbolt, J., "Nonlocal Microplane Model for Fracture, Damage, and Size Effect in Structures," *Journal of Engineering Mechanics*, ASCE, V. 116, No. 11, Nov. 1990, pp. 2484-2504.
37. Caner, F. C., and Bažant, Z. P., "Microplane Model M7 for Plain Concrete: II. Calibration and Verification," *Journal of Engineering Mechanics*, ASCE, V. 139, No. 12, 2013, pp. 1724-1735. doi: 10.1061/(ASCE)EM.1943-7889.0000571
38. Bažant, Z. P., and Oh, B. H., "Crack Band Theory for Fracture of Concrete," *Materials and Structures (RILEM, Paris)*, V. 16, No. 3, May 1983, pp. 155-177.
39. Červenka, J.; Bažant, Z. P.; and Wierer, M., "Equivalent Localization Element for Crack Band Approach to Mesh-Sensitivity in Microplane Model," *International Journal for Numerical Methods in Engineering*, V. 62, No. 5, 2005, pp. 700-726. doi: 10.1002/nme.1216
40. Li, K. K. L., "Influence of Size on Punching Shear Strength of Concrete Slabs," MEng dissertation, Department of Civil Engineering and Applied Mechanics, McGill University, Montréal, QC, Canada, 2000, pp. 26-44.
41. Birkle, G., "Punching of Fat Slabs: The Influence of Slab Thickness and Stud Layouts," PhD dissertation, Faculty of Graduate Studies, University of Calgary, Calgary, AB, Canada, 2004, pp. 63-71.
42. CEB-*fib* Bulletin No. 12, "Punching of Structural Concrete Slabs," Technical Report, Fédération internationale du béton, 2001, pp. 250-307.
43. Bažant, Z. P., and Le, J.-L., "Probabilistic Mechanics of Quasibrittle Structures: Strength, Lifetime, and Size Effect," Chapter 3, Cambridge University Press, Cambridge, UK, pp. 35-57.